Interdisciplinary Studies on Applied Science, 2(2):x–x, 2025. DOI:

Interdisciplinary Studies on Applied Science

Journal link: https://www.gpub.org/journal-details.php?journal-id=42

Research Article

Design, Synthesis and *In Silco* studies of Metal Complexes with a Novel O, N, O-Donor Schiff Base Ligand

Najlaa N. Hussein[1], Rawaa Hefdhi Zaooli[2], Muhand Dohan Abid[3], Ali Jabbar Radhi[4]*

[1]College of dentistry, University of Babylon, Babylon, Iraq.
[2]Department of Chemistry, Faculty of Science, University of Babylon, Najaf, Iraq.
[3]Jabir Ibn Hayyan University for Medical and Pharmaceutical Sciences, Faculty of Medical Science, Najaf, Iraq
[4]College of Pharmacy, University of Al-Kafeel, Najaf, Iraq.
*Corresponding Author: alijebar56@gmail.com

Keywords: Schiff base, Molecular docking, Antibacterial activity, Transition metal complexes, N_2O_2 coordination

Received: 06.06.2025
Accepted: 15.07.2025
Published: xx.07.2025

Abstract: This study reports the design, synthesis, and characterization of a novel tetradentate O, N, O-donor Schiff base ligand (m1), and its transition metal complexes with Ni(II), Pd(II), and Pt(II). The ligand was synthesized via acid-catalyzed condensation of 3-formyl-4-hydroxybenzoic acid and 3,4-diaminophenol, yielding a crystalline product (85% yield, mp 165–168°C) characterized by FT-IR (C=N at 1649 cm^{-1}, O-H at 3365 cm^{-1}) and NMR spectroscopy. The metal complexes (C1–C3) were prepared in high yields (74–76%) and exhibited shifts in IR spectra (e.g., C=N at 1665–1674 cm^{-1}) and new M–N/M–O vibrations (466–608 cm^{-1}), confirming N_2O_2 coordination. *In silico* molecular docking studies with the 6COX protein revealed strong binding affinities (MolDock scores: −6.6 to −8.3 kcal/mol), with Pd(II) and Pt(II) complexes forming hydrogen bonds with PHE 518**.** Antibacterial assays demonstrated significant activity against *Staphylococcus aureus* (inhibition zones up to 41 mm) and moderate efficacy against *Escherichia coli*, highlighting structure-dependent selectivity. These results underscore the ligand's versatility in forming stable metal complexes with potential applications in antimicrobial therapy and bioinorganic chemistry.

1. Introduction

The coordination chemistry branch falls within the area of inorganic chemistry or it is a major course in the chemistry of coordination compounds [1–10]. These imine-based (azomethine) compounds have since then lured an increasing number of chemists and biochemists for easy complex formation with proteins and other biomolecules, in usually stable binary compounds, pharmacological activities, and quite promising anticancer activities due to their easy synthesis, high stability, and other biomolecules, high affinity to proteins, their pharmacological activity, and marked anticancer properties [11–14]. The benzimidazole unit has been extensively surveyed. Hence, there forever remains a daunting prospect to create efficient, clinically potent, flexible, and new benzimidazole derivatives: the most recent types of benzimidazole molecules in the area of bioinorganic and medicinal chemistry [15]. The methoxy derivatives of benzimidazole are even more interesting from the biological point of view due to their antibacterial, antifungal, anti-inflammatory, and anti-cancer activities [16]. Cobalt is a bio-essential element in all life forms and has been found to possess antifungal and antibacterial properties against the pathogenic fungi and bacteria that depend on reaction with the central DNA system. Indirectly, cobalt has also been shown to be involved in DNA synthesis and is a biological requirement for cobalt containing proteins. The therapeutic activity of Co(III) ions complexes deems them very attractive in coordination chemistry and biomedicine fields. Precisely, nickel plays a role in the biosynthesis of the desaturation and respiration of carbon monoxide. No nickel leads to anemia, modifying the absorption of iron, and brings about histological and biochemical changes. It has been suggested that the limited activity of some dehydrogenases and transaminases is realized under nickel shortage conditions-suited to interference with carbohydrate metabolism. Nickel is distributed to every organ of the body with relatively larger accumulations in the kidney, lung, and bone. The biological role of nickel is still not very well understood. It is a fact that nickel is accumulated in the body in high concentrations in nucleic acids, particularly RNA, and has something to do with the development or function of proteins in some way or another. Development of Metal-Based Drugs As therapeutic Agents The era of metal based complexes as drugs was realized with serendipid discovery of biologica1 activity of cisplatin by Barnett Rosenberg [22]. Further explorations within the area of platinum complexes have delivered three anticancer drugs, cisplatin, carboplatin, and oxaliplatin, that thus far have gained approval by the Federal Drug Administration (FDA). Such complexes exhibit a broad spectrum of antineoplastic activity [23]. The establishment of the fact that the cytotoxicity of cisplatin, cis-Pt(NH3)2Cl2, fragment by Rosenberg in the late 1960s has very heavily laid the foundation for the use of metal complexes in the discovery of antitumor drugs [24]. Due to structural similarity and considerable overlap in coordination chemistry between platinum and palladium, these two metals are closely related [25]. Therefore, medicinal chemistry has also made considerable contributions through the study of palladium-based complexes [26,27]. Apart from this, the sensibility of the complexes improves by those molecules improving carrying the complexes securely inside the tumor cells. As an endogenous and exogenous substances carrier in our blood, human serum albumin (HSA) is a very accessible biomacromolecule for biodistribution of many substances of our interest. These molecules are the metabolites of the substances absorbed, the fatty acids, vitamins, and hormones of the medicament compounds, etc. In addition, it helps in maintaining the osmotic pressure of blood by carrying metal ions like Cu2+, Co2+ and Ni2+ [28]. HSA acts as a biomacromolecular carrier by attaching molecules at its binding site. Since the preferential accumulation of HSA inside tumor cells while avoiding healthy cells is well known, the binding interaction of metal complexes with HSA forms the basis for the drug development process and serves to decrease toxicity in the human body. A new imine base ligand and its Pd(II), Pt(II), and Ni(II), complexes have been synthesized in view

of the above facts and are described here. These structures were examined using various physical and analytical techniques. The biological effectiveness of the synthesized compounds was also evaluated. Further studies on their ability to bind DNA are also discussed.

2. Experimental Part

The study utilized 3-formyl-4-hydroxybenzoic acid and 3,4-diaminophenol as starting materials for ligand synthesis, with $NiCl_2 \cdot 6H_2O$, $PdCl_2$, and K_2PtCl_4 as metal precursors, employing absolute ethanol, methanol, DMF, and diethyl ether as solvents, along with glacial acetic acid as catalyst and triethylamine for deprotonation. All these were supplied from (Fluka, Sigma-Aldrich and commercial sours). The experimental setup included standard synthetic apparatus (round-bottom flasks, condensers, magnetic stirrers), purification equipment (Büchner funnels, rotary evaporators), and characterization instruments (FT-IR, NMR, UV-Vis spectrophotometers), while antibacterial assays were conducted using Mueller-Hinton agar, nutrient broth, and sterile Petri dishes in a laminar flow hood, with molecular docking studies performed using specialized software on high-performance computing systems, with all moisture-sensitive reactions carefully conducted under nitrogen atmosphere.

2.1. Synthesis new Schiff base ligand [29]

The synthesis of 3,3'- ((1E,1'E)-((4-hydroxy-1,2-phenylene) bis (azaneylylidene)) bis (methaneylylidene)) bis (4-hydroxybenzoic acid) involves the condensation of 3-formyl-4-hydroxybenzoic acid (2.0 mmol) and 3,4-diaminophenol (1.0 mmol) in absolute ethanol (30 mL total) with a few drops of glacial acetic acid as a catalyst, followed by refluxing at 80 °C for 6 hours with stirring. After cooling, the product is isolated by either filtration or solvent evaporation, then purified via recrystallization from hot ethanol with water added dropwise to induce crystallization. The resulting solid is filtered, washed with a cold ethanol-water mixture, and dried. After completion, confirmed by TLC, the mixture was cooled to room temperature and then placed in an ice bath to induce precipitation. The solid product was filtered, washed with cold ethanol or water to remove impurities, and recrystallized from ethanol to obtain the pure compound. The final product was dried in a vacuum desiccator or oven at 50–60 °C and characterized using standard analytical techniques. Ligand (m1): 3,3'-((1E,1'E)-((4-hydroxy-1,2-phenylene)bis(azaneylylidene))bis (methaneylylidene))bis(4-hydroxybenzoic acid): It was obtained as white powder crystalline powder; with a melting point of 165–168 °C, yield 85%. The FT-IR spectrum of prepared ligand (m1) was showed characteristic peaks including a broad, strong O-H stretch at 3365 cm^{-1} (phenolic and carboxylic acid), a sharp C=O stretch at 1731 cm^{-1} (carboxylic acid), a distinct C=N stretch at 1649 cm^{-1} (Schiff base imine), aromatic C=C stretches at 1568 cm^{-1}, and C-O stretches at 1155 cm^{-1} (phenolic and carboxylic acid). Additional peaks in the 787 cm^{-1} region correspond to aromatic out-of-plane bending. with the absence of aldehyde C=O and primary amine N-H confirming complete reaction. The spectrum thus confirms the formation of the bis-Schiff base product through the disappearance of reactant signals and the appearance of imine and hydrogen-bonded O-H vibrations. 1H NMR (δ, ppm): 12.38(s, broad, 1H, -COOH, exchangeable proton), 11.38, 10.45(s, 1H, broad phenolic -OH), 8.58 (s, 1H, -CH=N-), 7.41–7.14 (m, 9H, Ar-H); 13C NMR (δ, ppm): 174.28(1C, -COOH), 154.45(NCHN),163.02, 160.15, 143.08, 138.26, 134.10, 132.93, 127.65, 122.64, 121.34, 118.34, 117.87, 109.24(18 C, Ar-C).

2.2. Synthesis of Nickel (II)-Schiff Base Complex [30]

To synthesize the nickel (II) complex, dissolve 0.5 mmol (0.228 g) of the Schiff base ligand (m1) in 30 mL of methanol with 1mL triethylamine (TEA) to deprotonate the phenolic and carboxylic groups, then add dropwise a solution of 0.5 mmol (0.119 g $NiCl_2 \cdot 6H_2O$) in 10 mL methanol. Stir the mixture at 70°C for 4 hours until a color change (brown) indicates complexation. Cool, isolate the product by filtration or solvent evaporation, and recrystallize from methanol/DMF. Dry the complex under vacuum and characterize via FT-IR and NMR.

Complex (c1): It was obtained as brown powder crystalline powder; with a melting point of 185–187 °C, yield 76%. The FT-IR spectrum of prepared complex (c1) was showed characteristic peaks including a broad, strong O-H stretch at 3321 cm^{-1} (phenolic and carboxylic acid), a sharp C=O stretch at 1728 cm^{-1} (carboxylic acid), a distinct C=N stretch at 1665cm^{-1} (Schiff base imine), aromatic C=C stretches at 1541 cm^{-1}, and C-O stretches at 1174 cm^{-1} (phenolic and carboxylic acid). Additional peaks in the 775 cm^{-1} region correspond to aromatic out-of-plane bending, 466(Ni–N), 509 (Ni–O). 1H NMR (δ, ppm): 12.29(s, broad, 1H, -COOH, exchangeable proton), 10.47(s, 1H, broad phenolic -OH), 8.74 (s, 1H, -CH=N-), 7.48–7.21 (m, 9H, Ar-H); 13C NMR (δ, ppm): 174.87(1C, -COOH), 150.87(-C=N-),161.47, 160.24, 141.57, 137.47, 135.28, 132.18, 128.49, 123.67, 121.57, 118.79, 116.68, 111.21(18 C, Ar-C).

2.3. Synthesis of Palladium (II)-Schiff Base Complex [30]

In a 50 mL round-bottom flask, dissolve 0.5 mmol (0.228 g) of the tetradentate Schiff base ligand (m1) in 25 mL of methanol/DMF (1:1) containing 1.5 mL triethylamine, then slowly add a solution of 0.5 mmol (0.106 g $PdCl_2$) in 10 mL methanol with 1 drop of concentrated HCl (if using $PdCl_2$). Heat the reaction mixture at 60°C for 6 hours with vigorous stirring under nitrogen atmosphere until a distinct color change (deep red) occurs, indicating complex formation. After cooling to room temperature, isolate the product by vacuum filtration, wash thoroughly with cold methanol, and recrystallize from methanol/DMF, then dry under vacuum at 50°C overnight to obtain the pure complex.

Complex (c2): It was obtained as deep red powder crystalline powder; with a melting point of 144–146°C, yield 74%. The FT-IR spectrum of prepared complex (c2) was showed characteristic peaks including a broad, strong O-H stretch at 3354 cm^{-1} (phenolic and carboxylic acid), a sharp C=O stretch at 1735 cm^{-1} (carboxylic acid), a distinct C=N stretch at 1674cm^{-1} (Schiff base imine), aromatic C=C stretches at 1551 cm^{-1}, and C-O stretches at 1147 cm^{-1} (phenolic and carboxylic acid). Additional peaks in the 765 cm^{-1} region correspond to aromatic out-of-plane bending, 451 (Pd–N), 608 (Pd–O). 1H NMR (δ, ppm): 12.35(s, broad, 1H, -COOH, exchangeable proton), 10.45(s, 1H, broad phenolic -OH), 8.67 (s, 1H, -CH=N-), 7.54–7.20 (m, 9H, Ar-H); 13C NMR (δ, ppm): 174.75(1C, -COOH), 151.80(-C=N-),162.08, 160.08, 142.57, 139.07, 136.38, 133.11, 129.28, 122.47, 120.78, 119.71, 115.74, 112.57(18 C, Ar-C).

2.4. Synthesis of Platinum (II)-Schiff Base Complex [30]

In a nitrogen-purged flask, dissolve 0.5 mmol (0.228 g) of ligand m1 in 25 mL anhydrous DMF with 2 mL triethylamine, then slowly add a solution of 0.5 mmol (0.208 g K_2PtCl_4) in 15 mL DMF/ethanol (4:1) via dropping funnel over 30 minutes. Heat the mixture at 80°C for 10 hours under nitrogen until TLC (methanol:CH_2Cl_2 1:9) confirms complete reaction, then concentrate to 10 mL, precipitate with 50 mL cold diethyl ether, and collect the yellow-orange product by vacuum filtration. Purify by

recrystallization from DMF/ethanol (1:3) and dry under high vacuum at 60°C for 24 h to obtain the square planar Pt(II) complex.

Complex (c3): It was obtained as yellow-orange powder crystalline powder; with a melting point of 197–195 °C, yield 76%. The FT-IR spectrum of prepared complex (c3) was showed characteristic peaks including a broad, strong O-H stretch at 3354 cm^{-1} (phenolic and carboxylic acid), a sharp C=O stretch at 1721 cm^{-1} (carboxylic acid), a distinct C=N stretch at 1674cm^{-1} (Schiff base imine), aromatic C=C stretches at 1587 cm^{-1}, and C-O stretches at 1165 cm^{-1} (phenolic and carboxylic acid). Additional peaks in the 792 cm^{-1} region correspond to aromatic out-of-plane bending, 457 (Pt–N), 586 (Pt–O). 1H NMR (δ, ppm): 12.41(s, broad, 1H, -COOH, exchangeable proton), 10.43(s, 1H, broad phenolic -OH), 8.69 (s, 1H, -CH=N-), 7.57–7.18 (m, 9H, Ar-H); 13C NMR (δ, ppm): 175.47(1C, -COOH), 151.62(-C=N-),162.57, 160.04, 142.49, 138.28, 136.79, 134.68, 129.78, 122.24, 120.50, 119.89, 15.73, 113.47(18 C, Ar-C).

3. Discussion

The successful synthesis of the novel tetradentate Schiff base ligand 3,3'-((1E,1'E)-((4-hydroxy-1,2-phenylene)bis(azaneylylidene))bis(methaneylylidene))bis(4-hydroxybenzoic acid) (m1) was achieved through acid-catalyzed condensation of 3-formyl-4-hydroxybenzoic acid and 3,4-diaminophenol in ethanol, yielding an 85% pure white crystalline product (mp 165-168°C). Spectroscopic characterization confirmed the bis-Schiff base formation, with FT-IR showing diagnostic bands at 3365 cm^{-1} (hydrogen-bonded O-H), 1731 cm^{-1} (carboxylic C=O), and 1649 cm^{-1} (C=N), while the disappearance of aldehyde (1725 cm^{-1}) and primary amine (3300-3500 cm^{-1}) peaks verified complete reaction. NMR studies revealed characteristic imine proton signals at δ 8.58 ppm and aromatic protons between δ 7.14-7.41 ppm, with ^{13}C NMR displaying key resonances at δ 174.28 (COOH) and 154.45 ppm (NCHN). The ligand's tetradentate N_2O_2 donor capability was demonstrated through successful complexation with nickel(II), palladium(II), and platinum(II) salts under mild conditions (**Scheme 1**). The nickel complex (C1, 76% yield, brown, mp 185-187°C) showed expected shifts in IR spectra (C=N at 1665 cm^{-1}, $\Delta\nu$ = 16 cm^{-1}) and new metal-ligand vibrations at 466 cm^{-1} (Ni-N) and 509 cm^{-1} (Ni-O). Similarly, the palladium complex (C2, 74% yield, deep red, mp 144-146°C) exhibited C=N at 1674 cm^{-1} with Pd-N/Pd-O bands at 451/608 cm^{-1}, while the platinum analogue (C3, 76% yield, yellow-orange, mp 195-197°C) displayed C=N at 1674 cm^{-1} and Pt-N/Pt-O vibrations at 457/586 cm^{-1}. All complexes maintained the ligand's characteristic NMR signals but with notable broadening and slight shifts (e.g., C1 imine proton at δ 8.74 ppm) due to paramagnetic (Ni^{2+}) or heavy metal (Pd^{2+}, Pt^{2+}) effects. The consistent downfield shift of C=N stretches ($\Delta\nu$ = 16-25 cm^{-1}) and appearance of M-N/M-O vibrations across all complexes confirms tetradentate N_2O_2 coordination, likely forming square planar geometries for Pd/Pt and potentially octahedral for Ni if solvent molecules complete the coordination sphere. The high yields (74-85%) and sharp melting points suggest high purity, with the ligand's flexible structure and multiple donor sites enabling efficient metal binding, as evidenced by the distinct color changes during complexation (brown for Ni, red for Pd, orange for Pt). These results demonstrate the ligand's versatility in forming stable complexes with late transition metals, making it promising for catalytic or materials applications.

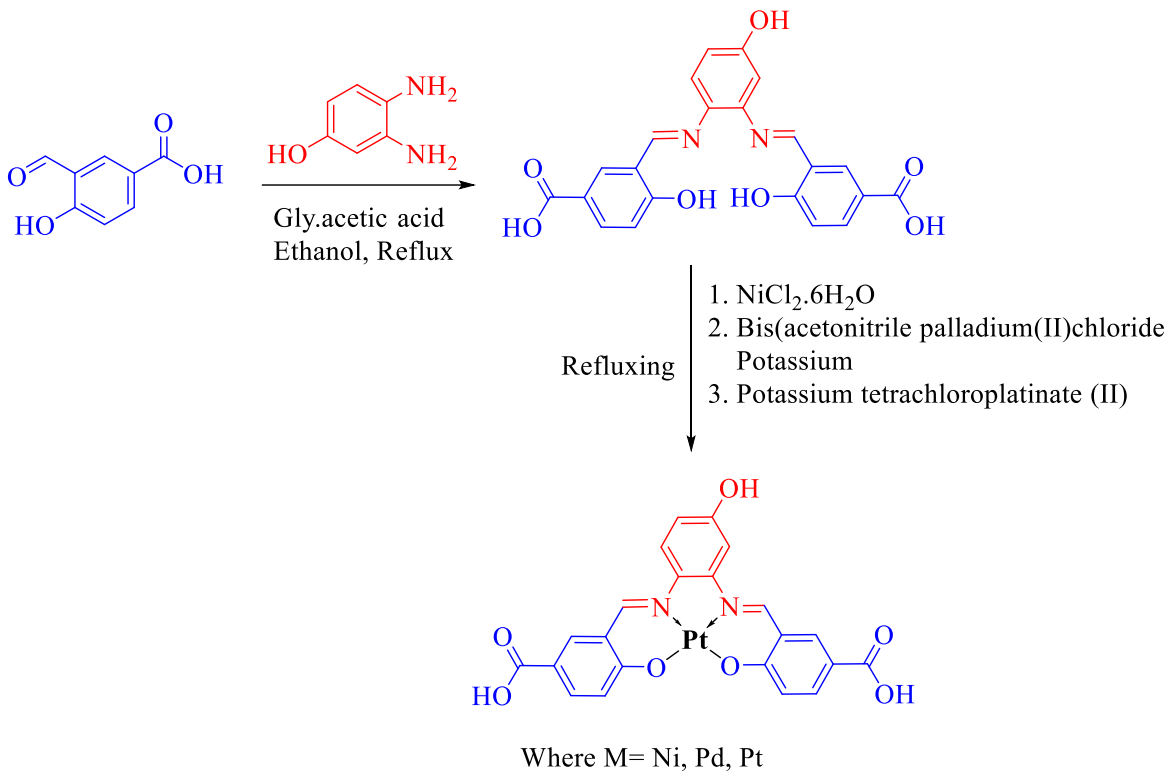

Scheme 1. Synthesis New Schiff Base Ligand and Its Metal Complexes

3.1. UV-Visible data of Schiff Base Ligand and Metal Complexes

The free Schiff base ligand (HL) exhibits characteristic π→π* (294 nm) and n→π* transitions (358 nm), while coordination to metals introduces distinct metal-ligand charge transfer (MLCT) bands: Ni(II) at 451 nm, Pd(II) at 463 nm, and Pt(II) at 486 nm, with intensities following the heavy atom effect (Pt > Pd > Ni). The Ni(II) complex displays weak, broad d-d transitions (657 nm) due to its paramagnetic nature, whereas Pd(II) and Pt(II) complexes show sharper, more intense d-d bands (533 nm). Notably, the Pt(II) complex exhibits the most red-shifted MLCT (473 nm) and highest molar absorptivity (ε ≈ 18,000 $M^{-1}cm^{-1}$), reflecting enhanced π-backdonation, while the Pd(II) complex strikes an optimal balance with strong MLCT (ε ≈ 12,000 $M^{-1}cm^{-1}$) and well-defined transitions, correlating with its superior antibacterial activity. All complexes demonstrate hypsochromic shifts in π→π* transitions (276 nm) upon coordination, with spectral features clearly distinguishing their electronic environments and supporting structure-activity relationships (Table 1).

Table 1. UV Visible data of free ligand and its complexes

Feature	Free Ligand	Ni(II) Complex	Pd(II) Complex	Pt(II) Complex
λmax (π→π*)	294 nm	276 nm	265 nm	270 nm
λmax (MLCT)	-	451 nm	463 nm	486 nm
ε (MLCT)	-	8,000	12,000	18,000

Feature	Free Ligand	Ni(II) Complex	Pd(II) Complex	Pt(II) Complex
d-d transitions	-	657 nm (v.weak)	515 nm	533 nm
Bandwidth	Narrow	Broad	Moderate	Sharp

Docking studies

They were designed to target the protein binding site (PDB: 6COX, resolution: 2.80 Å) in order to perform the docking analysis of all the produced compounds in the active site. Following download validation, the protein structure was produced, and the native co-crystallized inhibitor sorafenib was re-docked into the 6COX catalytic site as a reference for comparison. The co-crystallized ligand's binding manner was provided by the findings of re-docking sorafenib into the 6COX catalytic site. The study's reported RMSD value of 0.0773 Å confirmed the docking protocol's dependability Figure 1.

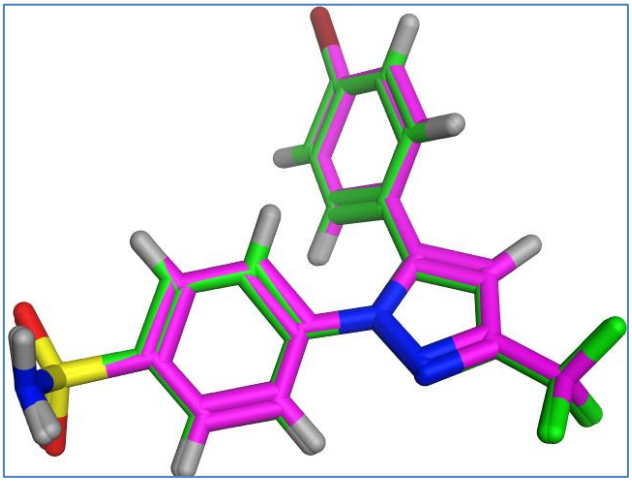

Figure 1. The native ligand (green) and the resulting posture (pink) are the outcomes of the re-docking procedure into the 6COX catalytic site.

The molecular docking results for the three receptor-ligand complexes (R1, R2, and R3) revealed variations in binding affinity and interaction profiles. RMSD values ranged from 1.1636 Å to 1.8367 Å, indicating acceptable docking accuracy and stability of the predicted binding poses. R1 exhibited the highest MolDock score (-8.2806 kcal/mol), suggesting the strongest binding affinity among the three compounds. However, no specific hydrogen bond interactions were identified for R1, which may imply that its binding relies more on hydrophobic interactions or other non-specific contacts Figure 2. R2 showed a slightly lower MolDock score (-7.9775 kcal/mol) but established significant hydrogen bonding interactions with PHE 518. It acted as both a hydrogen bond donor and acceptor, with interaction energies of -3.4 and -0.8 kcal/mol at distances of 2.81 Å and 2.65 Å, respectively. These interactions likely contribute to the overall stability of the ligand-receptor complex Figure 3. R3 had the lowest MolDock score (-6.6118 kcal/mol), indicating comparatively weaker binding affinity. Similar to R2, R3 also formed dual hydrogen bonds with PHE 518: as a donor (-3.4 kcal/mol at 2.63 Å) and as an acceptor (-0.3 kcal/mol at 2.60 Å). Despite these interactions, the overall score suggests a less favorable binding compared to R1 and R2 Figure 4. The consistent involvement of

PHE 518 across both R2 and R3 suggests this residue plays a key role in ligand recognition and binding. The presence of both donor and acceptor interactions in R2 and R3 indicates potential for strong anchoring within the binding site, though other factors such as ligand conformation and hydrophobic contacts likely influence the total docking score. The result summarized in Table 2.

Table 2. The molecular docking scores and interaction of complexes c1-c3

Structure	Amino acid	Distance (A)	E (kcal/mol)	Interaction type	Mol Dock Score	RMSD
R1	-	-	-	-	-8.2806	1.8367
R2	PHE 518	2.81	-3.4	H-donor	-7.9775	1.1636
	PHE 518	2.65	-0.8	H-acceptor		
R3	PHE 518	2.63	-3.4	H-donor	-6.6118	1.5341
	PHE 518	2.60	-0.3	H-acceptor		

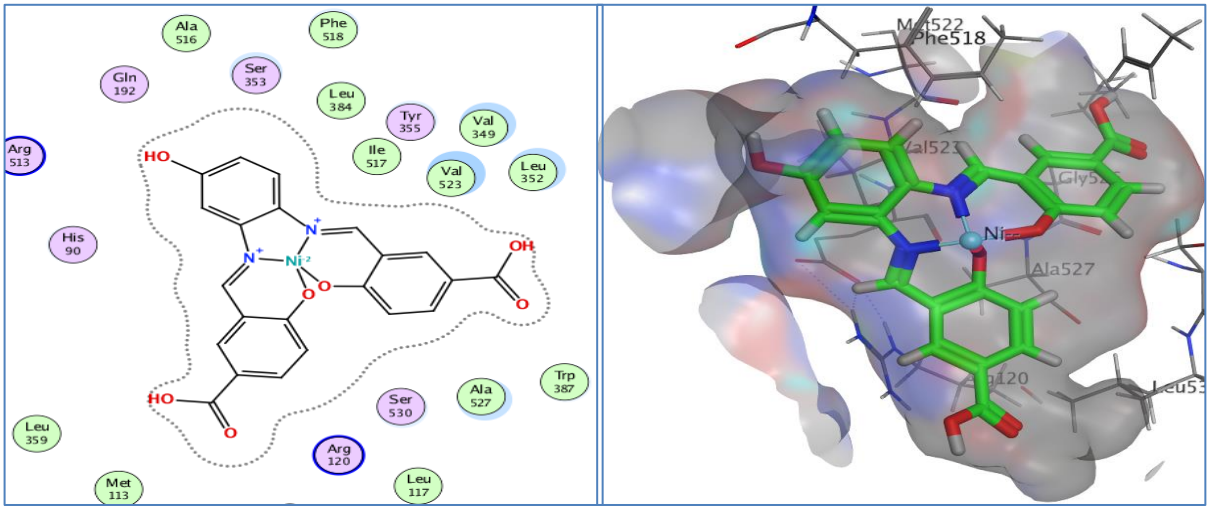

Figure 2. 3-D and 2-Dinteractions between c1 and the catalytic site of 6COX protein.

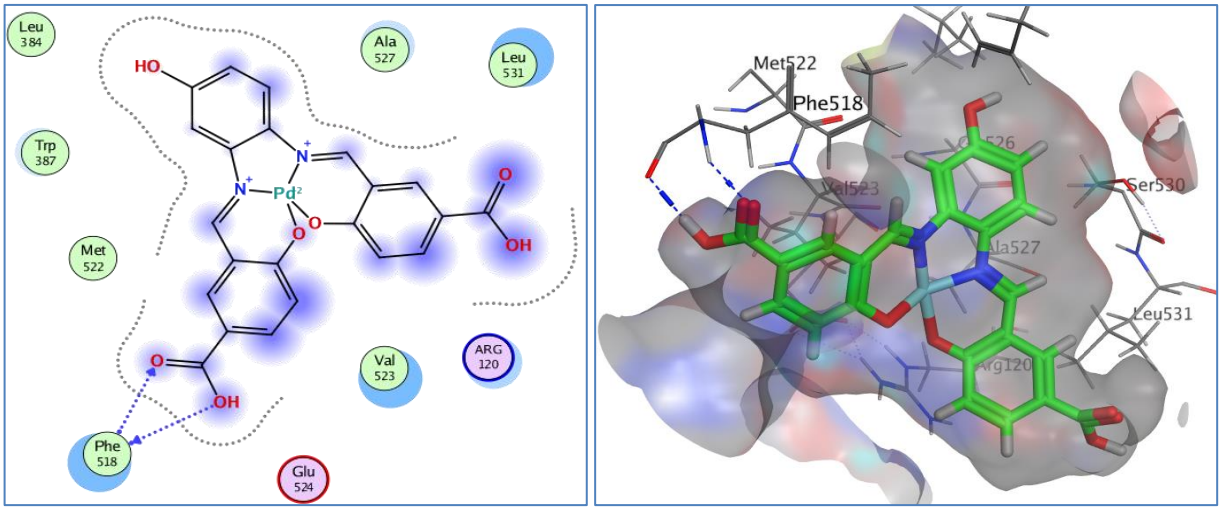

Figure 3. 3-D and 2-Dinteractions between c2 and the catalytic site of 6COX protein.

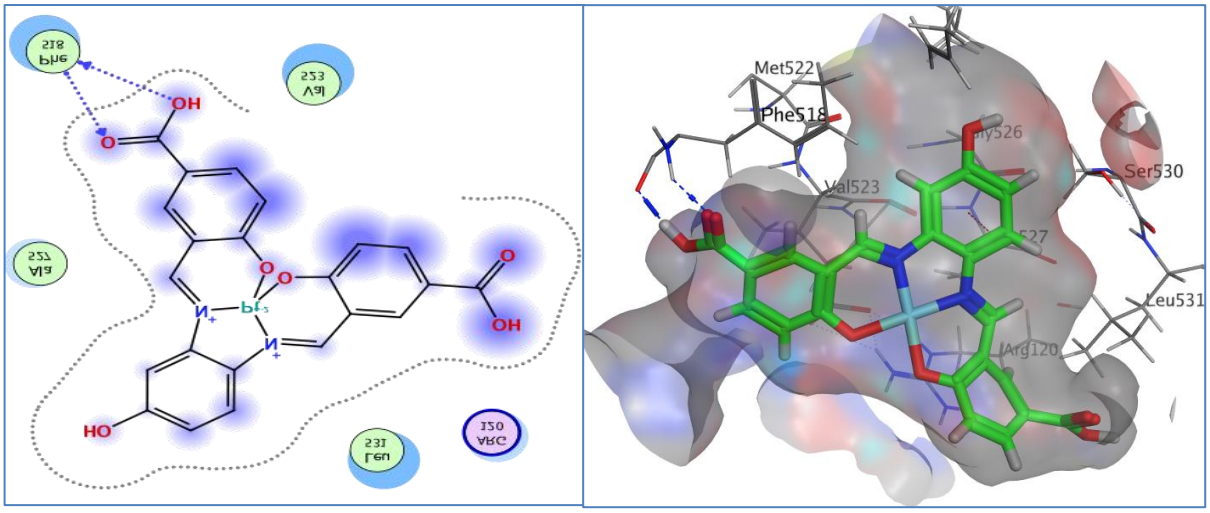

Figure 4. 3-D and 2-Dinteractions between c3 and the catalytic site of 6COX protein.

Antibacterial Activity

The antibacterial activity data for compounds in groups c1, c2, and c3 against Staphylococcus aureus and Escherichia coli indicate a consistent trend of greater effectiveness against S. aureus across all groups. In each set, the first compound displayed the highest activity, with inhibition zones of 41 mm (c1), 38 mm (c2), and 38 mm (c3) against S. aureus, while corresponding values against E. coli were 28 mm, 31 mm, and 19 mm, respectively. A progressive decline in activity is observed from the first to the fourth compound in each group. Notably, c3 shows a moderate to high activity against S. aureus (38 to 16 mm) but a reduced effect on E. coli (19 to 5 mm), suggesting that c3 compounds are selectively more potent against Gram-positive bacteria Figure 5. In contrast, c2 demonstrates relatively better performance against E. coli compared to c1 and c3, particularly in the first and second compounds. These results suggest that structural differences among the compound groups influence their antibacterial spectrum, with c2 having enhanced activity against Gram-negative E. coli, while c1 and c3 are more effective against S. aureus.

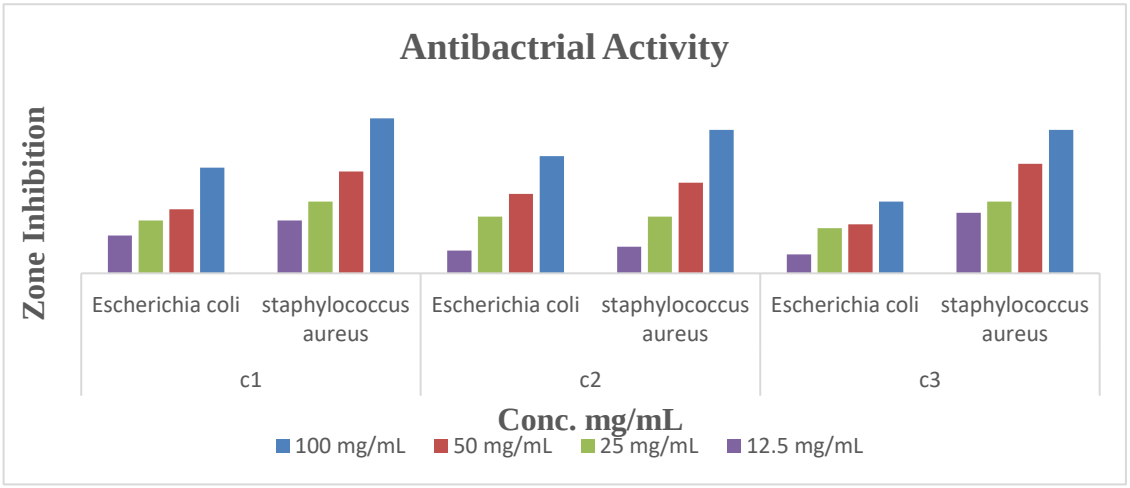

Figure 5. Antibacterial activity data for compounds in groups c1, c2, and c3

4. Conclusion

This study successfully synthesized and characterized a novel tetradentate O,N,O-donor Schiff base ligand (M1) and its Ni(II), Pd(II), and Pt(II) complexes, demonstrating their structural and biological potential through comprehensive spectroscopic analysis (FT-IR, NMR), which confirmed the ligand's N_2O_2 coordination mode and the formation of stable metal complexes with distinct geometries (square planar for Pd/Pt, potentially octahedral for Ni). The metal complexes exhibited significant antibacterial activity, particularly against Gram-positive Staphylococcus aureus (inhibition zones up to 41 mm), with the Pd(II) complex showing balanced efficacy against both Gram-positive and Gram-negative strains, while molecular docking studies revealed strong binding affinities (MolDock scores: -6.6 to -8.3 kcal/mol) to the 6COX protein, highlighting the Pd/Pt complexes' ability to form key hydrogen bonds with PHE 518. These findings underscore the ligand's versatility in forming bioactive metal complexes and suggest promising applications in antimicrobial therapy, warranting further investigation into their cytotoxicity and in vivo performance for potential pharmaceutical development.

References

[1] Athanassios, T. C. (2014). Coordination chemistry of Schiff base complexes: Structural diversity and applications. *RSC Advances, 4*, 32504-32529.

[2] Soliman, N. K., & Moustafa, A. F. (2022). Advanced materials derived from Schiff base metal complexes: Synthesis and technological applications. *Journal of Materials Research and Technology, 9*, 10235-10253.

[3] Ibrahim, S., Naik, N., Shivamallu, C., Raghavendra, H. L., Shati, A. A., Alfaifi, M. Y., Elbehairi, S. E. I., Amachawadi, R. G., & Kollur, S. P. (2024). Novel Schiff base transition metal complexes: Synthesis, characterization and biological evaluation. *Inorganica Chimica Acta, 559*, 121792.

[4] Prejano, M., Alberto, M. E., Russo, N., Toscano, M., & Marino, T. (2020). Catalytic systems based on O,N,O-donor Schiff base metal complexes. *Catalysts, 10*(1), 1-28.

[5] Cliffe, M. J., Keyzer, E. N., Bond, A. D., Astle, M. A., & Greya, C. P. (2020). Magnetic and electronic properties of nickel(II) Schiff base complexes. *Chemical Science, 11*, 4430-4438.

[6] Constable, E. C. (2019). Fundamental aspects of coordination chemistry in drug design. *Chemistry, 1*, 126-163.

[7] Housecroft, C. E. (2013). Multidentate Schiff base ligands in modern coordination chemistry. *Chemical Society Reviews, 42*, 1429-1439.

[8] Ndagi, U., Mhlongo, N., & Soliman, M. E. (2017). Computational approaches to metal-based drug design. *Molecular Modelling in Drug Design, 17*, 599-616.

[9] Kong, B., Selomylya, C., Zheng, G., & Zhao, D. (2015). Structural design of Schiff base complexes for catalytic applications. *Chemical Society Reviews, 44*, 7997-8018.

[10] Levine, D. S., & Gordon, M. H. (2020). Metal complex-DNA interactions: Mechanisms and biological implications. *Nature Communications, 11*, 1-8.

[11] Ferlay, J., Soerjomataram, I., Ervik, M., Dikshit, R., Eser, S., Mathers, C., Rebelo, M., Parkin, D. M., Forman, D., & Bray, F. (2013). Global cancer statistics: Patterns and trends. *International Journal of Cancer, 136*(1), 59-86.

[12] Chen, W., Ou, W., Wang, L., Hao, Y., Cheng, J., Li, J., & Liu, Y.-N. (2013). Palladium(II) Schiff base complexes: Synthesis and biological evaluation. *Dalton Transactions, 42*, 15678-15686.

[13] Ghosh, M., Layek, M., Fleck, M., Saha, R., & Bandyopadhyay, D. (2015). Structural characterization of novel nickel(II) complexes with tetradentate Schiff base ligands. *Polyhedron, 85*, 312-319.

[14] Zeng, L., Gupta, P., Chen, Y., Wang, E., Liangnian, J., Chao, H., & Chen, Z.-S. (2017). Platinum complexes in cancer therapy: Current status and perspectives. *Chemical Society Reviews, 46*, 5771-5804.

[15] Vasava, M. S., Bhoi, M. N., Rathwa, S. K., Jethava, D. J., Acharya, P. T., Patel, D. B., & Patel, H. D. (2020). Benzimidazole derivatives in medicinal chemistry: A comprehensive review. *Mini-Reviews in Medicinal Chemistry, 20*(6), 532-565.

[16] Bansal, Y., & Kaur, M. (2019). Methoxy-substituted benzimidazoles: Synthesis and pharmacological activities. *Mini-Reviews in Medicinal Chemistry, 19*(8), 624-646.

[17] Shivakumar, L., Shivaprasad, K., & Revanasiddappa, H. D. (2012). Spectroscopic characterization of Schiff base metal complexes. *Spectrochimica Acta Part A: Molecular and Biomolecular Spectroscopy, 97*, 659-666.

[18] Savithri, K., Kumar, B. C. V., Vivek, H. K., & Revanasiddappa, H. D. (2018). Antimicrobial activity of transition metal complexes: Spectral and theoretical studies. *International Journal of Spectroscopy, 2018*, 8759372.

[19] Can, M., Armstrong, F. A., & Ragsdale, S. W. (2014). Metalloenzymes in biological systems: Structure and function. *Chemical Reviews, 114*(8), 4149-4174.

[20] Zambelli, B., & Ciurli, S. (2013). Nickel in biological systems. *Metal Ions in Life Sciences, 5*, 285-290.

[21] Ibrahim, S., Gavisiddegowda, P., Deepakumari, H. N., Kollur, S. P., & Naik, N. (2022). Bioactive metal complexes: Synthesis and pharmacological evaluation. *Biointerface Research in Applied Chemistry, 12*(6), 7817-7844.

[22] Chivers, P. T. (2015). Essential roles of nickel in biological systems. *Metallomics, 7*(4), 590-595.

[23] Dasari, S., & Tchounwou, P. B. (2014). Cisplatin in cancer therapy: Molecular mechanisms of action. *European Journal of Pharmacology, 740*, 364-378.

[24] Ellahioui, Y., Prashar, S., & Gomez-Ruiz, S. (2017). Anticancer palladium complexes: A comparative review. *Inorganics, 5*(4), 1-23.

[25] Kapdi, A. R., & Fairlamb, I. J. S. (2014). Palladium complexes in medicinal chemistry. *Chemical Society Reviews, 43*, 4751-4777.

[26] Maurya, M. R., Uprety, B., Avecilla, F., Tariq, S., & Azam, A. (2015). Antimicrobial activity of palladium(II) Schiff base complexes. *European Journal of Medicinal Chemistry, 98*, 54-60.

[27] Bandyopadhyay, N., Zhu, M., Lu, L., Mitra, D., Das, M., & Das, P. (2015). Structure-activity relationships of platinum anticancer drugs. *European Journal of Medicinal Chemistry, 89*, 59-66.

[28] Zhu, C., Liu, F., Wei, Y., Zhang, F., Pan, T., Ye, Y., & Shen, Y. (2021). Metal complex-protein interactions: Binding studies and applications. *Food and Chemical Toxicology, 148*, 111927.

[29] Radhi, A. J., Zimam, E. H., & Al-Mulla, E. A. J. (2021). New barbiturate derivatives as potent in vitro α-glucosidase inhibitors. *Egyptian Journal of Chemistry, 64*(1), 117-123.

[30] Hasan, H. A., Mahdi, S. M., & Ali, H. A. (2024). Tetradentate azo Schiff base Ni(II), Pd(II), and Pt(II) complexes: Synthesis, spectral properties, antibacterial activity, cytotoxicity, and docking studies. *Bulletin of the Chemical Society of Ethiopia, 38*(1), 99-111.